Article:
Haruna, MA, Pervaiz, S, Hu, Z et al. (2 more authors) (2019) Improved rheology and high-temperature stability of hydrolyzed polyacrylamide using graphene oxide nanosheet. Journal of Applied Polymer Science, 136 (22). 47582. ISSN 0021-8995

https://doi.org/10.1002/app.47582

Improved rheology and high-temperature stability of hydrolysed polyacrylamide using graphene oxide nanosheet

Maje Alhaji Haruna[1], Shahid Pervaiz[1], Zhongliang Hu[1], Ehsan Nourafkan[1], Dongsheng Wen[1, 2]*

[1]School of Chemical and Process Engineering, University of Leeds, Leeds, U.K.

[2]School of Aeronautic Science and Engineering, Beihang University, Beijing

*Tel: +44(0)113 343 1299; Email: d.wen@leeds.ac.uk and d.wen@buaa.edu.cn

Abstract

Hydrolysed polyacrylamide is a polymer that extensively used in chemical industry and hydrocarbon extraction and refinery processes, but suffers a common problem of high-temperature instability. This study improved high-temperature rheological characteristics of hydrolysed polyacrylamide (HPAM) by using novel graphene oxide (GO) nanosheets. Stable GO dispersions in aqueous HPAM were formulated, and their dynamic and viscoelastic behaviours were studied. The results showed that the addition of GO significantly increased the viscosities and high-temperature stability of the base polymer fluid, as well as the elastic properties of the dispersion. Spectral data indicated the formation of covalent linkages and electrostatic hydrogen bonding between the GO and the HPAM functional groups, leading to enhanced stability and viscosity that is beneficial for high-temperature oil recovery.

1. INTRODUCTION

Enhanced Oil Recovery (EOR) is a popular technique for increasing the amount of extracted crude oil from the oilfield. Polymer flooding (PF) is the most common technique for EOR application. This method operates by reducing the mobility of the aqueous phase, thereby enhancing the sweep effectiveness [1-2]. Among the many different types of water-compatible polymers that are commonly used in polymer EOR, hydrolysed polyacrylamide (HPAM) is the most frequently used in field applications [1]. In addition to its relevance for this application, HPAM has found to be used in many other fields, including in wastewater treatment from oil extraction [2] as well as in a low-grade oil sand [3]. The rheological properties of water can be altered significantly by the addition of HPAM. This can lead to repulsion between the extremely high molecular weight of polymers and the negative charges along the polymer chain [4]. HPAM has featured in a considerable number of related polymer tests [5].

Although PF EOR techniques are widely considered for EOR application, harsh reservoir conditions such as high temperature, high pressure and/or high salinity can cause degradation of the polymer [6]. It is observed that HPAM would undergo a significant reduction in viscosity and a decrease in the percentage of oil recovery in most of the high-temperature reservoirs [7]. The viscosity reduction could arise because of the effect of hydrophobic impairment due to an increase in the polymer mobility and the eventual damage of inter-chain linkages [8, 9]. When reservoir temperatures go above 60 °C, it is most likely that the acrylamide functionality would undergo hydrolysis to form acrylate derivatives [6] or carboxylic acid [10] groups, which have high affinity to salts in the reservoir. Also, the presence of any sodium ions can neutralise the negative charges, which can cause the shrinkage of the polymer chains and a consequent decrease of the hydrodynamic radius. The addition of NaCl solution can enhance the ionic strength of the system, leading to the compression of the double electrical layers (EDL) on HPAM molecular chains. The electrostatic repulsion among the anions would be also altered. The addition of $CaCl_2$ was reported to significantly decrease the viscosity of the HPAM as well as it pseudo plasticity due to the presence of the doubly charged cations [11]. Increasing the degree of hydrolysis causes the HPAM to precipitate from the bulk phase due to the formation of the complexes between the divalent cations and the polymer [12].

Moreover, prevention of the mutual repulsion that can exist between carboxylic groups on the backbone of the HPAM would lead to a shrinkage of the hydrodynamic volume, and subsequently more viscosity reduction [11, 13]. From another point of view, the many challenges that HPAM solutions could encounter in EOR applications could range from thermal challenges, leading to low thermal stability to tolerate severe reservoir conditions, leading to early degradation, or mechanical challenges, leading to inadequate durability and toughness. Other challenges could be related to

swelling, leading to deficient swelling ability or elasticity challenges, leading to insufficient, required viscoelasticity properties.

When attempting to address the multiple problems of polymer EOR, polymeric nanocomposites with highly dispersed inorganic particles have recently featured in the literature. [14-20]. In these processes, the addition of nanoparticles can directly affect the melt [21, 22], as well as the solution [18, 23] viscosities and rheological behaviours of the polymeric matrices. Different nanoparticles such as silica [24-26], carbon nanotubes [27], layered double hydroxide [28-30], nanoclay [18, 31], and metal oxides have all been investigated with regards to enhancing the rheological characteristics of polymers used in EOR applications.

In this work, attention was given to the use of graphene oxide (GO) as a reinforcing nanofiller in polyacrylamide. GO, is recognised for its distinguished mechanical, thermal and electrical characters [32]. Recently, Liu et al. have assembled GO/PAM nanocomposites by binding the surface of GO with the PAM chains via hydrogen bonding [33]. A chemically cross-linked composite of GO/PAM with enhanced mechanical strength was constructed by Shen et al. [34]. The characteristic nature of GO to generate self-assembled network when combined with the physical cross-linker species have led to their application in various systems [35, 36]. GO and reduced graphene oxide (RGO) i.e. deoxygenated graphene sheets have been also applied as physical cross-linkers, in such a way of eradicating the high demand of chemical cross-linking materials [33, 34]. Graphene flakes have been used by Fan et al. in enhancing the mechanical properties of chemically cross-linked polyacrylic acid (PAA) [37]. In advanced drilling fluid GO is also used as an additive for fluid-loss control [38], as a viscosity modifier for EOR [39] or as a crude oil/water emulsion systems stabiliser. Although previous research [33, 34] proclaimed the use of GO as a reinforcing nanofiller of PAM, but PAM itself has less tolerance to high salinity and high temperature (HSHT) compared to the HPAM. However, some pioneered work [24] reported that SiO_2 nanoparticles can improve the HPAM stability at (HSHT) condition, and no work reported using HPAM with GO under HSHT condition. Also large amount of SiO_2 is required (around 1 wt. %) to achieve a higher viscosity of HPAM [24]. Similarly, SiO_2 particles tend to agglomerate or even precipitate if they are not dispersed very well [40], and it may take longer time to get a well-dispersed mixture of SiO_2 and HPAM, which greatly decrease nanoparticles potential for field application [41].[2]. However, due to its two dimensional (2D) geometry, GO can provide a significant increase in viscosity and thermal stability of polymer matrix [42, 43]. This reduced the amount of nanoparticles required to reach a target viscosity for polymer flooding EOR and hence lower down the cost, and at the same time reduces the pore blockage causes by particle aggregation.

In this work, we propose a novel idea where GO nanosheet can be used as filler to form non-covalent bonds with HPAM. This assembly enhances the rheological properties of HPAM, by increasing their

overall EOR performance at high temperature and in high salinity reservoirs. For this purpose, a modified Hummers' method was used to synthesise a stable GO nanosheet from graphite powder. The rheological properties of formed nanocomposite were investigated under different temperatures and different salinity conditions. The long-term stability of the composites has been evaluated. A mechanistic view of the reinforced rheology is proposed based on elemental analysis.

2. MATERIAL AND METHODS

Hydrolysed polyacrylamide (HPAM) was provided by SNF FLOERGER, France, having a molecular weight of 10 mDa and a density of 0.9 g/cm^3. Sodium chloride with the purity of around 99.0% was purchased from Sigma-Aldrich.

2.1. Synthesis and characterisation of graphene oxide

Modified Hummers' method was used to synthesise a stable graphene oxide [44]. Graphite powder, hydrogen peroxide (H_2O_2, 36%) and potassium permanganate ($KMnO_4$, 99%) were purchased from Sigma-Aldrich. Nitric acid (HNO_3, 69%) and sulphuric acid (H_2SO_4, 95%) were obtained from VWR Chemicals. Graphite powder (less than 20 µm in size) was used as the starting material. A mixture of sulfuric acid and nitric acid was used for oxidation of graphite powder in water-based solution. In a typical synthesis, 12 grams of graphite powder was prepared in a mixture of 100 ml H_2SO_4 and 50 mL HNO_3 and stirred for 24 hours at room temperature. 100 ml of DI water was subsequently added to the mixture and then stirred continuously for another day. $KMnO_4$ (12 grams) was added slowly in the solution keeping the temperature of the mixture low. This was followed by stirring for five hours. 60 ml of 36% H_2O_2 was added in an ice bath to keep the temperature low, and this suspension was stirred overnight. The resultant suspension was filtered using a Whatman filter paper. The filtrate was then washed three times with 10% HCl, centrifuged (13000 rpm for 1 hour) and the supernatant was discarded. Morphologies of the fabricated GO nanosheets were determined by transmission electron microscopy and scanning electron microscope (TEM, FEI Tecnai TF20, and SEM, Hitachi SU8230 FESAM, Leeds LEMAS centre, Leeds, UK, respectively). UV-Vis spectrophotometer (UV-1800, Shimadzu, Kyoto, Japan) was used to determine the particle concentration based on Beers-Lambert law. Zeta potential was measured following dilution of the GO solution at $25 \pm 0.5^{\circ}C$ using a Malvern nanosizer based on dynamic light scattering (DLS) methods.

2.2. Composites preparation

To prepare the GO/HPAM composites, different concentrations (0.01, 0.02, 0.0.4, 0.06, 0.08 and 0.1 wt. %) of the GO sheets suspension were separately added dropwise into the designed HPAM solution under gentle stirring at room temperature, for example the ratio of HPAM/GO/water is 1:2:100 when 0.05 wt.% of HPAM and 0.1 wt.% of GO were dispersed in water. The GO/HPAM suspension was continually mixed by gentle stirring using a magnetic stirrer (SB 162-3, Stuart) for 24 hours to allow sufficient time for the GO to form a network with the graft polymer to achieve a stable composite material. Different brine concentrations were then added to the individual solutions followed by a further 24 h stirring at room temperature to investigate the effect of electrolytes. Table 1 shows the elemental compositions for HPAM, GO and HPAM/GO samples analysed by SEM-EDS.

Table 1. Summary of elemental compositions for dried HPAM, GO and HPAM/GO samples

	Elemental composition (%)			
Samples	C (%)	O (%)	N (%)	S (%)
HPAM	64.54	23.25	10.42	1.79
GO	59.47	40.25	0.00	0.28
HPAM_GO mixture	40.10	46.54	9.84	3.52

2.3. Characterization and stability test

The stability of the composites samples was investigated using a vertical scan analyser Turbiscan MA 2000 (Formulation, Toulouse, France), following the procedure explained by Hebishy et al. [45]. In each case, a cylindrical glass tube containing the suspension was used. The FTIR spectra of vacuum-dried HPAM, GO, and HPAM/GO composites samples was analysed using Fourier transform infrared (FTIR, PerkinElmer) spectrometer. The data were collected at a spectral resolution of 4 cm^{-1} within the scanning range of 4000−400 cm^{-1}. The XRD analysis was carried out on dried samples to evaluate the degree of polyacrylamide intercalation between the GO layers, using a Bruker D8 X-ray diffraction, fitted with a Cu Kα radiation (1.54 A˚, 40 kV, 40 mA). Data was collected from 2θ angle ranging of 10 – 70° with step size of 0.0495° at 35 s per step. pH of the dispersion was measured on a METTLER TOLEDO pH meter (seven Compact S210).

2.3.1. Rheological measurements

A TA discovery hybrid rheometer (DHR-2) from TA Instruments was used with a cone-and-plate geometry for both shear and dynamic rheological measurements. The gap was pre-set to the standard 0.052 millimetres. Steady and dynamic measurement observed to analyse the rheological behaviours of the suspensions which were of different concentrations. Advanced Peltier system was used to control the temperature. To minimise water evaporation while measurements, a plastic ring solvent trap was used to cover around the measuring geometry. The steady shear sweep was used to investigate the flow property of the material by recording the viscosity (η) versus shear rates ($\dot{\gamma}$) from 100 to 1000 s^{-1}. The dynamic frequency sweep was measured in the linear viscoelastic regions of the materials under shear-rate-controlled mode to find the viscoelastic behaviour of the composites in which the storage modulus (G') and the loss modulus (G") were measured at a range of angular frequency.

2.3.2. Long-term thermal stability

Pure HPAM and HPAM/GO nanocomposites samples were aged in an oven at 80 °C for the long-term thermal stability analysis. At different time intervals spanning 30 days, the viscosity of the samples was measured at 85 °C.

3. RESULTS AND DISCUSSIONS

3.1. Characterization and stability

The TEM images show typical wrinkles and a crumble-like structure of GO **(Fig. 1a)**, the selected area of electron diffraction (SEAD), as shown in **Fig. 1b** indicates that a clear diffraction brightness and spotty rings that indexed to a hexagonal crystal structure of graphite. The SEM images show that the surface of GO is smooth, indicating that the GO nanosheet is attached **(Fig. 1c). Fig. 1d** shows that the GO exhibit strong ultra-violet light absorption and a clear absorption at 280 nm. **Fig. 2a** depicts the X-ray diffraction (XRD) pattern of the HPAM, GO and the dried HPAM/GO composites. The XRD spectra were measured in a range from 5 to 70° **(Fig. 2a).** The XRD spectrum of HPAM shows the amorphous structure, while the XRD pattern of GO show (002) diffraction peak at 26.3° and another one at 43.2, indicating the distance between graphene layers. A bump between 2θ values of 24–28 suggests the presence of a few layered graphene. It is believed that these two peaks may have resulted from the restacking of graphene sheets [46-48]. The main peak at around 10.5° shows the formation of GO structure. Also, at around 26 and 43, two distinct diffraction peak was shown for the GO samples

diffractograms, representing (002) and (001) planes of GO respectively [49-51]. The results reveal the degree of exfoliation observed from XRD is coordinated by the functional group's interactions in the neighbouring GO sheets even though side interactions along the carboxyl terminal groups are also possible, revealing the formation of GO [51]. Contrarily, the nanocomposites of GO/HPAM exhibit several diffraction peaks at 30.5, 39.8, 56.5 and 65.25°, which confirmed the formation of stable GO/HPAM composites. These peaks correspond to the (220), (111), (511) and (440) planes of centred cubic lattice, revealing the existence of hexagonal and cubic phases in the composites. Considering the fact that HPAM is amorphous material, the appearance of sharp, strong peaks in the composites confirmed the product were crystallized. The Raman spectrum of HPAM, GO, and HPAM/GO composites are shown in **Fig. 2c,** GO spectrum demonstrated a D-band at 1357 cm^{-1} and a G-band at 1591 cm^{-1} respectively. The D-band is linked with the structural deformity relevant to the partly disorganised network of graphitic domains or generated by the functional group's attachments on the carbon basal plane. While the G-band is referred to the E2g mode first order scattering. The HPAM showed a tiny symmetrical band centred at around 481 cm^{-1} due to skeletal deformation [52] and a wide sloppy band at 1667 cm^{-1} due to the amide 1 vibration.

Similarly, there is a change in the frequency of amide II (primarily -NH_2 bending) from 1600 cm^{-1} to 1625 cm^{-1}**.** The changed of the amide I frequency indicates the formation of hydrogen bonding between two polymer chains [52]. However, the GO D-band and G-band become broadened in the HPAM/GO composite becoming more prominent and wide, indicating a considerable interaction between HPAM and GO.

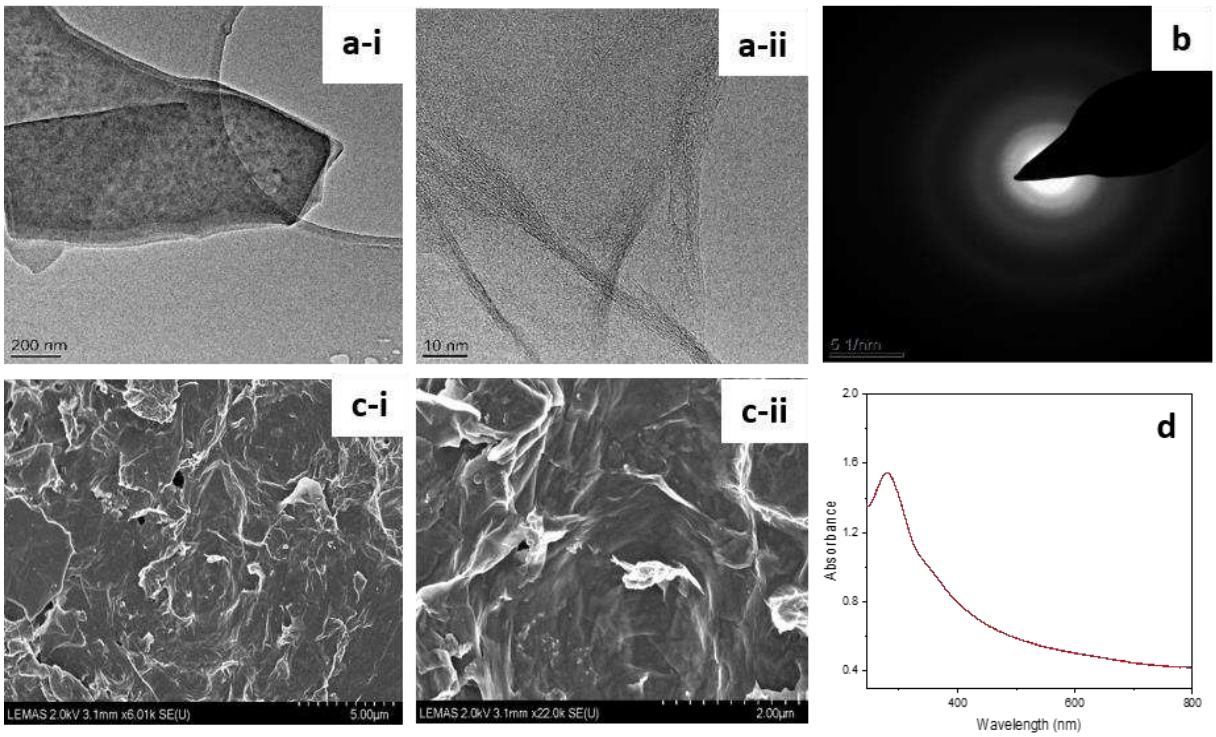

Figure 1. (a) TEM images (b) SAED (c) SEM images (d) the UV-vis spectrum of Go nanosheets

The essence of the chemical bonding structure between the HPAM and GO was evaluated using FT-IR spectroscopy to understand the formation mechanisms of GO/HPAM composite as shown in **Fig. 2b.** For HPAM spectrum, 1117, 1449, and 2953 cm^{-1} correspond to ring structure vibration of C-O-C stretching, methyl C-H bend, and C-H stretching vibration respectively. The peaks observed at 3321 and 2923 cm^{-1} can be attributed to the carbonyl and the amino group of the HPAM amides chain. The peaks at 1700 cm^{-1}.is attributed to the C=O (carbonyl functional group) stretching vibration while peak at 3424 cm^{-1} is related to the N-H stretching vibration. The amide I and amide II vibrational bands appear at 1650 and 1548 cm^{-1} [53]. The GO sheets FT-IR spectrum shows bands at 3420, 1395.5 and 1069.7 cm^{-1} which are referred to the symmetric and asymmetric stretching vibration of O-H, the bending vibration of O-H and the stretching vibration of the C-O bond in epoxide group, respectively [54, 55]. For HPAM/GO composites, the formation new peak at 1660 cm^{-1} demonstrated that the GO -COOH was transformed into $-COO^-$ with $-NH_3^+$ of HPAM as the counter-ions. Other than electrostatic interaction, hydrogen bonds also formed between the epoxy groups and OH of GO, and $-NH_2$ and C-O of HPAM presence in the composite material. In GO the epoxide group C–O stretching (1069.7 cm^{-1}) became weaker gradually and the GO OH bending peaks (1395.5 cm^{-1}) shifted to the higher wavenumber, confirming the existence of hydrogen bonds. The same peaks observed at 3321, and 2923 cm^{-1} in the HPAM spectrum were also shown in the HPAM/GO spectrum but was shifted to lower wavenumber (3302 and 2859 cm^{-1}), indicating stable dispersion of GO/HPAM nanocomposites. New peaks appear in HPAM/GO at 1081 and 1451 cm^{-1} which were not observed concerning the pure HPAM are due to the formation of C-O-C stretching ring structure vibration and methyl C-H bending vibration, respectively. These might be due to the of hydrolysable covalent cross-links formation between HPAM and GO [24, 56]. Besides, in GO/HPAM hybrid spectrum another peak appears at 2953 cm^{-1}, which indicates the formation of C-H stretching vibration, confirming the formation of covalent bond between carbon present in the GO backbone and hydrogen from the amide group of HPAM.

Moreover, the formation of N-H group at 3228 cm^{-1} in the composites spectrum is as a result of electrostatic interaction between the polar hydrogen in the GO and highly electronegative nitrogen atom present in the HPAM amide, which covalently bound to form hydrogen bond and further increases the hybrid suspension stability. Also, the absorption band formed at 1741 cm^{-1} is ascribed to carbonyl stretching vibration, the bands at 1568 cm^{-1} are responsible for $–CO-NH_2$ bonds and a band at 1376 cm^{-1} represent the C-N stretching vibration. Accordingly, the –CO-N-H mode contributes for the C-N stretching vibration and N-H bending vibration, which emerges from bonding between the amide group of HPAM chains and carboxylic group of the GO.

NMR spectroscopy was also employed aiming to present the confirmation that HPAM molecules were incorporated into GO sheets using Advanced 500 nuclear magnetic resonance spectrometer (Bruker Company, Ettlingen, Germany) in deuterium oxide (D_2O). **Fig. 3a and 3b** show ^{1}H-NMR of HPAM and HPAM/GO respectively. For pure HPAM, the absorption peaks at 1.407, 2.113 and 3.321 ppm represent -CH_2 protons. C-H and R-CO-NH_2 where denoted in the absorption peaks of 6.868 and 7.609 ppm, respectively. All of these indicated that the major polyacrylamide functional groups are found in the spectrum [57-59]. Compared to HPAM/GO spectrum, the -NH_2 and -CH_2 peaks in HPAM become broader and wide indicating modification in HPAM backbone after interacting with GO sheet, however, there are existence of new peaks marks with the different shapes and symbols at 6.873 ppm for Ar-OH and 3.639 ppm representing R-CO-NH_2 which certainly indicated how oxygen atom in GO interact with -NH_2 of HPAM to form hydrogen bond. The emergence of this new characteristic attraction peaks proves the successful grafting of HPAM chains onto the GO sheets.

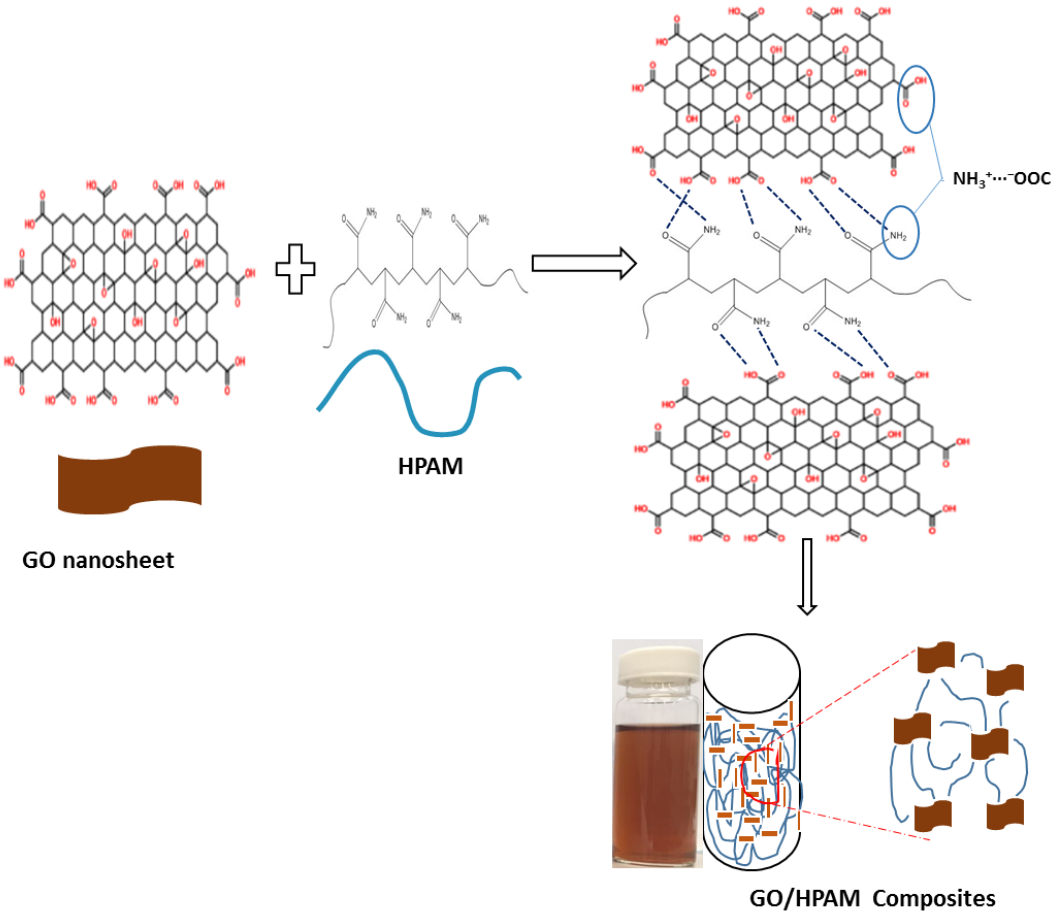

Scheme 1. Schematic representation of the network structure of GO/HPAM composites.

Considering the FT-IR, Raman and XRD observations, a proposed mechanistic illustration of GO/HPAM nanocomposite is shown in **scheme 1**. The numerous functional groups containing oxygen (carboxyl, hydroxyl, and epoxide groups and so on) were on the edges and basal planes of GO nanosheet. After interacting with the HPAM, the -COOH group presence in the GO can protonate HPAM $-NH_2$ group to generate the pairs of $-NH_3^+\cdots{}^-OOC-$ ion. Similarly, three sort of hydrogen bonds were also observed in the composites in addition to the electrostatic interaction, viz: among the HPAM carboxyl groups and GO hydroxyl groups, and the remaining two prevailed midway around the protonated $-NH_3^+$ of HPAM together with the GO epoxy groups and carboxyl groups, respectively, as proved by FT–IR analysis. Remarkably, the results suggested the evolution of chemical ligation between HPAM segments and GO in the nanocomposites. However, the composites were observed and considered as stable enough to circumvent the possible phase separation that can easily happen in the fabrication of the nanocomposites via physical mixing of the polymer and GO.

Table 2: Zeta potential of HPAM, GO and HPAM/GO nanocomposites at 70 °C for different pH

Concentrations	Zeta Potential (mV)
Pure HPAM	-45.1
Pure GO	-24.2
0.02 wt. % GO/HPAM	-50.5
0.04 wt. % GO/HPAM	-50.2
0.08 wt. % GO/HPAM	-47.1

The static position method is the most generally used method to decide the stability of nano composition. It allows the sample to stand in a container for a particular period, and the distance or colour difference in sedimentation was observed by the naked eye [60-62]. However, this method cannot evaluate the true stability of our composite suspensions. As shown in **Fig. 2d**, the sedimentation behaviour was monitored and recorded every 5 minutes for 2 hours using turbiscan analyser, backscattering intensity/transmission intensity profiles versus the sample height. The backscattering profiles interpretation explained the changes in the backscattering light caused by the particle sedimentation within the sample cell. Over the period, the change in backscattering varies with the sample height when sedimentation occurs. However, if the particle dispersion is stable, over the entire sample cell no noticeable change in the backscattering profiles is observed. The suspensions containing 0.01, 0.02, 0.04 and 0.08 wt. % GO respectively in HPAM/GO composites shows a representative example of a highly stable suspension **(Fig. 2d).** The results indicate that since there is no particle precipitation throughout the height of the container, no sedimentation takes place in all

range of GO concentrations. This improved stability is associated with the change of the particles surface charge. Therefore zeta potential was used to investigate the incorporated amount of GO state of the surface charge in the HPAM/GO composites and pure samples at 70 °C. The results in **Table 2** indicate negative zeta potential for all the measured samples showing improved stability. The zeta potential of the composites shows stronger intercalation between the HPAM and GO nanosheet, indicating that improved dispersion stabilisation has been achieved [57, 63].

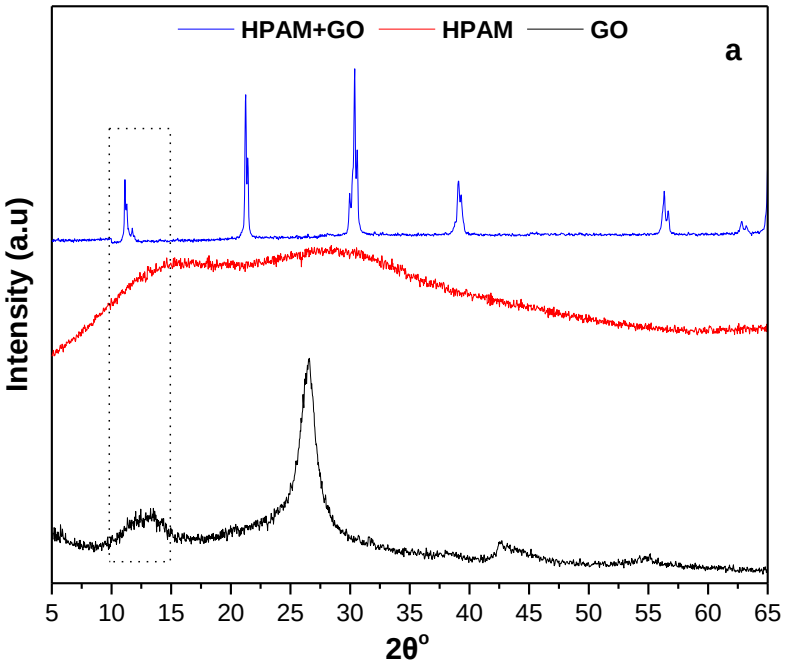

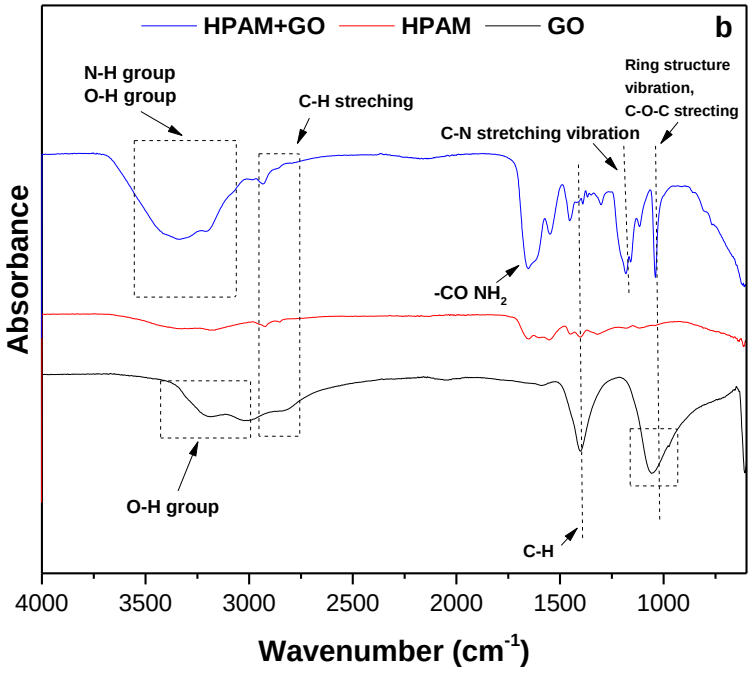

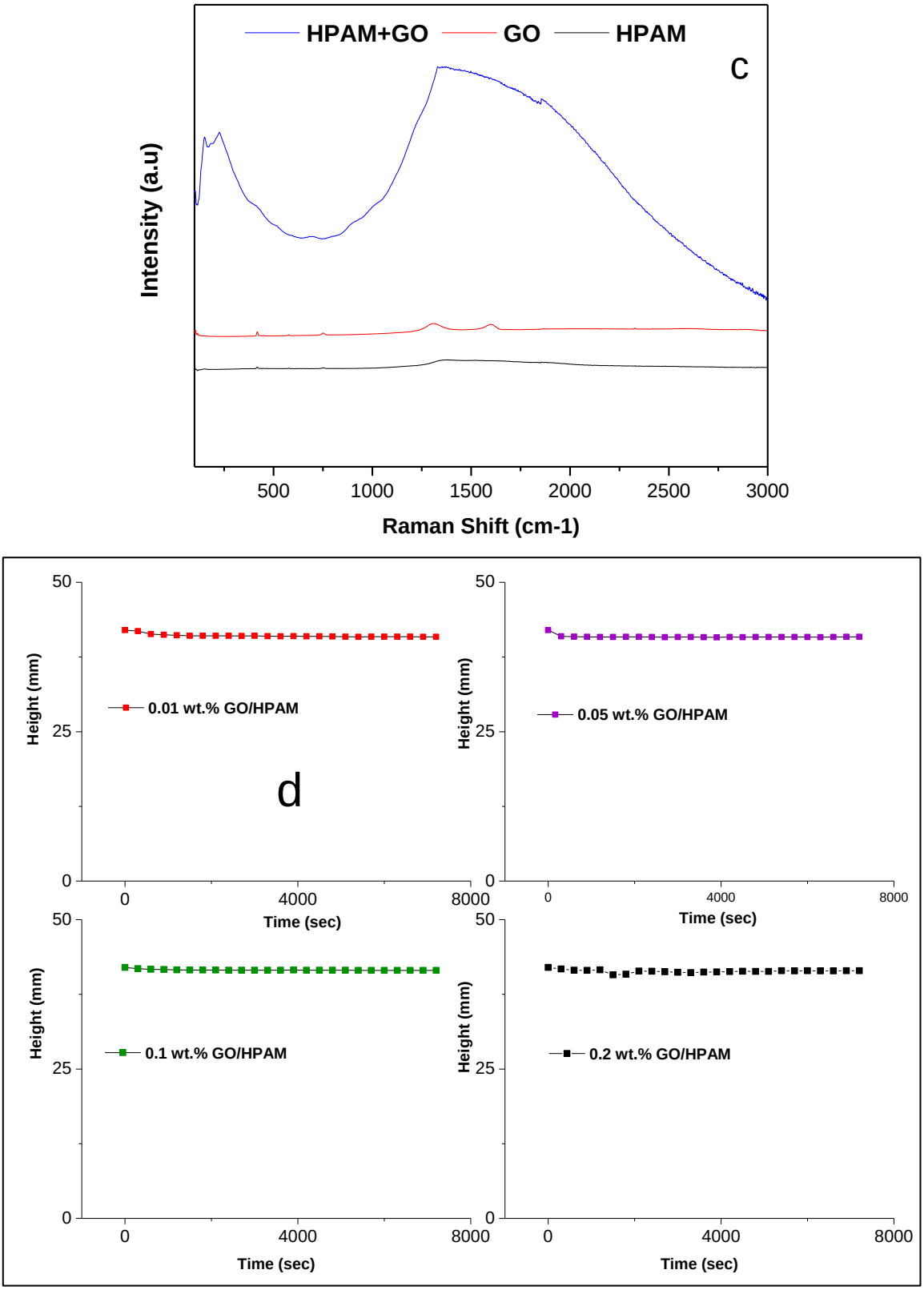

Figure 2. (a) XRD patterns for HPAM, GO and HPAM/GO composites (b) FTIR spectra for HPAM, GO and HPAM/GO composites (c) Raman Spectroscopy for HPAM, GO and HPAM/GO composites (b)

Turbiscan stabilization test for 2 hours duration with scan every 5 minute for HPAM, GO and HPAM with different loadings of the GO at 60 °C.

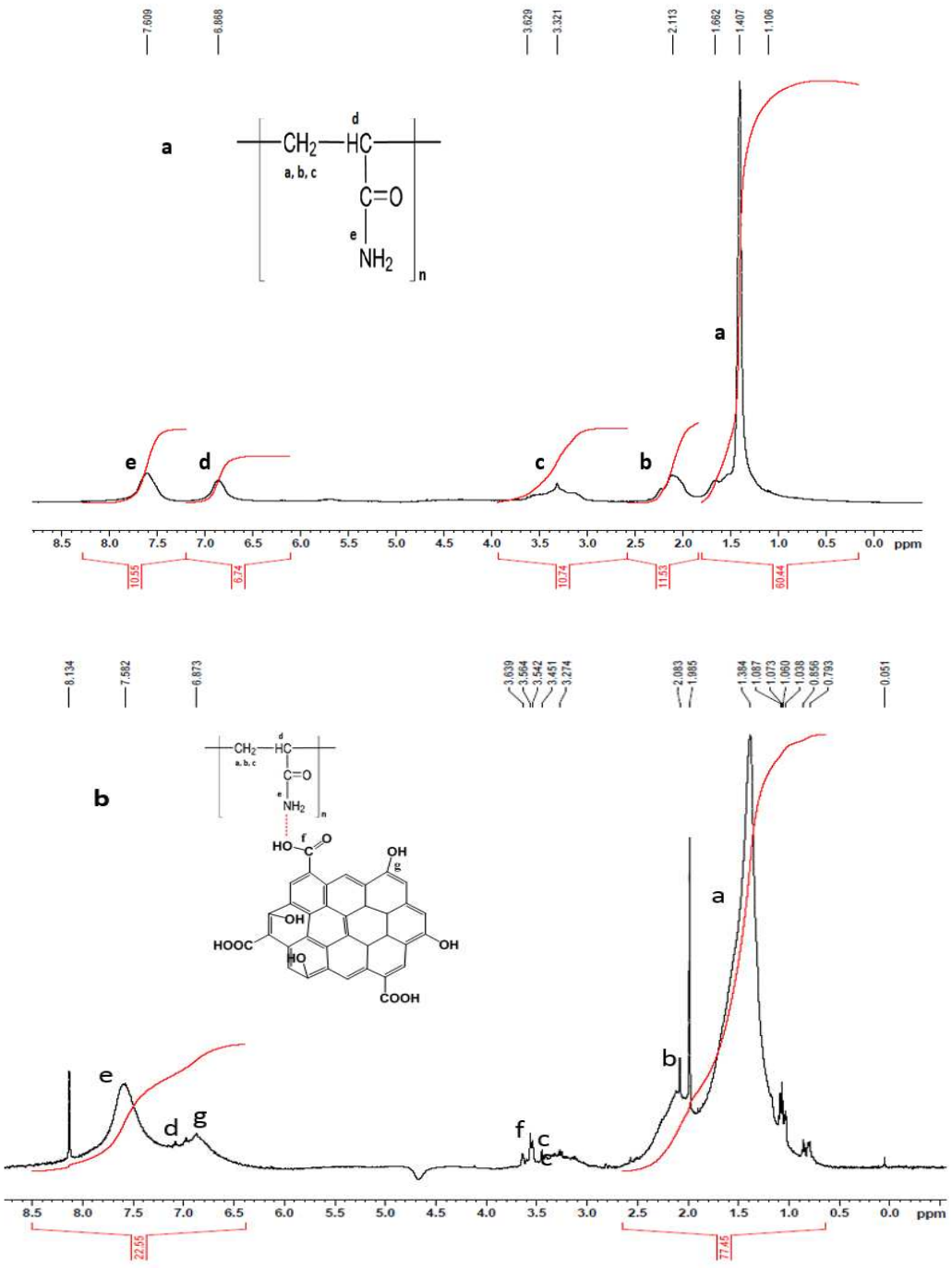

Figure. 3. ^{1}H-NMR for (a) HPAM and (b) HPAM/GO composites in D_2O

3.2. Rheological results

3.2.1. Critical association concentration

Polymer molecules can develop concentration-dependent association, which can occur mostly when mixing with other substances like surfactants and nanoparticles [24, 64]. This association can be apparent at the concentration of the first break, often termed the critical association concentration (CAC), where polymer molecules and other substances begin to associate. It is significant to know the CAC value to achieve required morphological features or specific modification of the polymer solution such as in a polymer/nanoparticle hybrid. However, the CAC value can be obtained using other approaches such as light scattering determination, variable view cell apparatus [64], and the changes in fluorescence characters when micellisation occurs [65].

Notwithstanding, HPAM solution rheological investigation at 25 °C was used, in this work, to determine the CAC. **Fig. 4** illustrates the 1000 shear viscosity versus HPAM concentration, and it can be observed that the curve is split into two parts, below 0.06 wt. % HPAM concentration, the viscosity patterns show slight differences with the increase in polymer concentration. For the concentration equal to and above 0.06 wt. %, the viscosity was sharply increased as HPAM concentration increases. This trend suggests that 0.06 wt. % is the HPAM CAC used in this study. As the polymer concentration increased, the number of molecules increased within the solution resulting in more significant interaction between the polymer chains, leading to greater frictional effect and subsequently alter the composites stability.

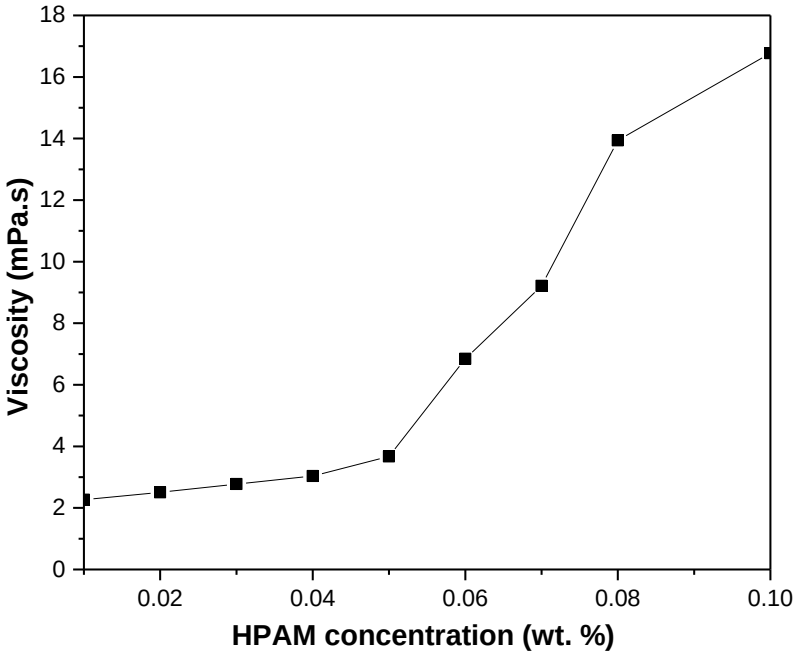

Figure 4. Viscosity as a function of HPAM concentration (25 °C and shear rate 1000 s^{-1})

3.2.2. Effect of nanoparticle concentration

As mention earlier, the intramolecular hydrophobic association can play a significant role when making polymer-nanoparticle hybrids because of the CAC of the polymer In this section, 0.05 wt. %, which was immediately below the CAC level, was used for investigating the impact of GO nanoparticle on the rheological properties of HPAM. Different GO concentration 0.01, 0.02, 0.04, 0.06, 0.08 and 0.1 wt. % were added into the solution containing 0.05 wt. % HPAM and their rheological behaviour were studied. **Fig. 5a and 5b** illustrate the dependence of the solution viscosity on the shear rate for the HPAM/GO hybrids at 25 and 85 °C, respectively. It can be seen from the graphs, the apparent viscosity decreases sharply with increasing shear rate from 100 to 1000 s^{-1} indicating a shear thinning behaviour for the entire system. Compared to the pure HPAM and low GO loading, solution with the high GO concentration shows better resistance to sear rate with less viscosity reduction as shear rate increases. The decrease in viscosity with shear rate may result from the slippage of HPAM chain on to the GO sheets platelets. The results show that the low viscosity of the solution at a high shear rate is due to the extension of the average distance from end to end, and as a result of disentanglement process of the polymeric chain when shearing. It can be viewed that, the shear thinning behaviour of the hybrids depends on the viscoelastic characteristics of the polymer matrix, which may emerge from the disintegration of HPAM/GO bridged at shear fields.

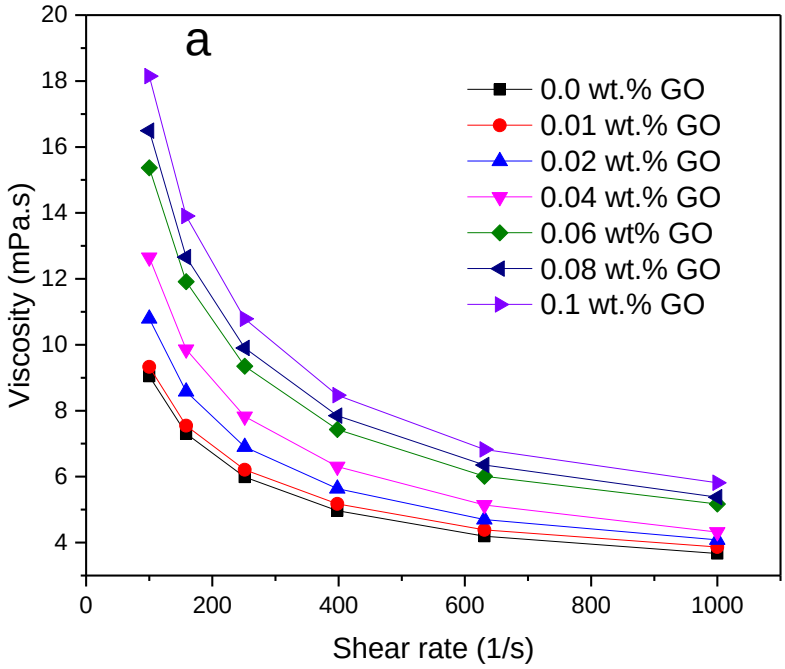

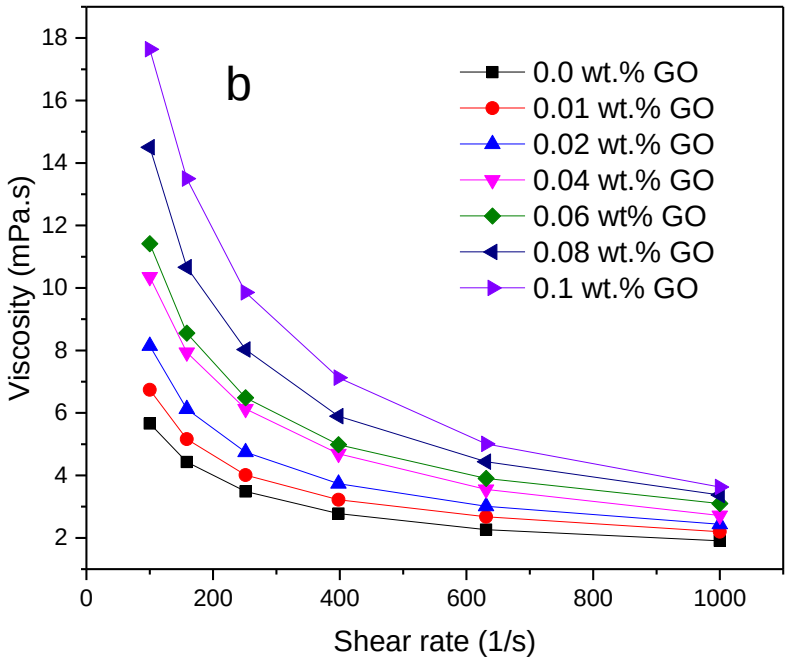

Figure 5. The dependence of viscosity for HPAM/GO nanocomposites on the shear rate with different GO loading ((a) T= 25 °C (b) T= 85 °C. and shear rate 100-1000 s^{-1}).

On the other hand, **Fig. 6** shows viscosity as a function of GO concentration for both 25 °C and 85 ^{0}C respectively. It is evident that the thickness of the hybrid increases with the increase in GO concentration. This result behaves the same trends with adding HPAM concentration, which shows the rapid growth in the viscosity as the concentration was increased. It can be observed that with the addition of 0.01 wt. % GO at 85 °C, the apparent viscosity of the HPAM increases by 13 % and correspondingly increases by 47% with the addition of 0.1 wt. % GO. While at 25 °C, the HPAM viscosity increases by 5% after adding 0.01 wt. % GO and then a 36 % increases were observed following the addition of 0.1 wt. % GO. The same concentration of GO was also dispersed in water, after measuring the viscosity, it was seen that with the addition of GO suspension in the water there are slight changes in the viscosity at both 25 and 85 °C respectively. These may be interpreted by the high water polarity such that when the GO nanoparticles are dispersed in water, the molecules of water covered the surface of the particles, and thus cause the suspension to retain most of it viscosity. The higher viscosity of HPAM/GO composites could arise as a result of the strengthened the polymer molecular weight, ductility, and embrittlement due to the formation of covalent linkages and electrostatic hydrogen bonding between the GO and the HPAM functional groups, leading to enhanced material stability and hence more viscosity enhancement as demonstrated by the FT-IR results. This increase in viscosity of HPAM with GO loading could be attributed to the large surface area of two-dimensional (2D) layer of the GO particle, this peculiarity lead to significant improvements of different properties

such as thermal stability of the polymer matrix following the insertion of very small content of the GO. Similar results were reported [42] for graphene-based poly(vinyl alcohol) composite and [43] for PAM/GO composites with the enhanced mechanical strength. Moreover, Hu et al., [24].observed similar viscosity increase with addition of SiO_2 nanoparticle in HPAM but with lower viscosity increase at an equivalent particle concentration.

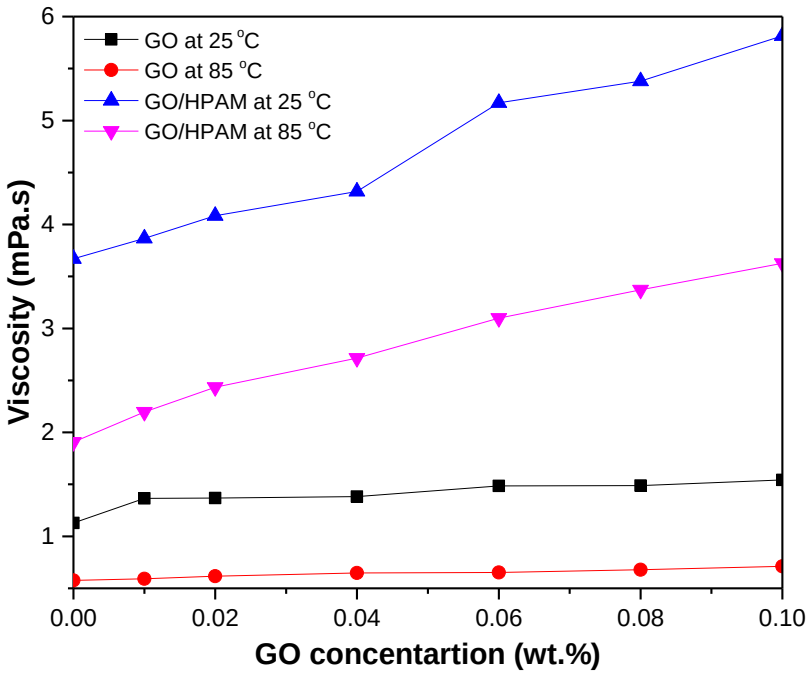

Figure 6. Viscosities of 0.05 wt. % HPAM with different GO loadings (T= 85 ˚C and 25 ˚C, and shear rate 1000 s^{-1}). Under the same experimental conditions, the viscosity for the neat 0.05 wt% HPAM was measured as 1.90759 mPa·s at 85 °C and 3.67055 mPa·s at 25 °C.

3.2.4. Effect of temperature on viscosity of HPAM/GO composites

Water-soluble polymers are susceptible to temperature. As heat is applied, the polymer chains can undergo chemical or physical changes, which can result in unwanted changes to the significant properties of the polymer, leading to polymer degradation. In many cases, molecular degradation often called thermal degradation occurs due to overheating, especially when the polymer is subjected to high temperature. The long chain molecular component of the polymer backbone begins to separate at high temperature which can eventually cause molecular scission. Typically at a specific temperature, the strength of the bonds deteriorates and causes the attached elements on the polymer to be detached. Because of this, we investigate how GO nanoparticle will influence the polymer stability at a different temperature, ranging from 25 to 85 °C. **Fig. 7** describes the apparent

viscosity as a function of temperature for the composites containing 0.05 wt. % HPAM/0.02 wt. % GO, the corresponding concentration of both pure HPAM and GO were also investigated. It shows that the viscosity of all the three samples decreased drastically with increasing temperature. This effect can also be seen when the viscosity curves of the pure HPAM and that of the HPAM/GO are compared such that a sharper in viscosity decrease is observed as the temperature rises indicating less tolerance to temperature. For a pure HPAM, the higher temperature would necessarily continue to break down intermolecular hydrophobic associations changing the HPAM backbone and then hydrolyse its acrylamide group into acrylate groups. Hence more viscosity reduction for HPAM solutions. It can also be seen in **Fig. 7** that, in the case of the pure GO, increasing the temperature the decrease in viscosity is not as much as pure that HPAM. This could be the reason why HPAM/GO composites acquired more viscosity than sole HPAM because of the strong thermal stability of GO, and probably due to the coupling of the network linkage between GO to HPAM.

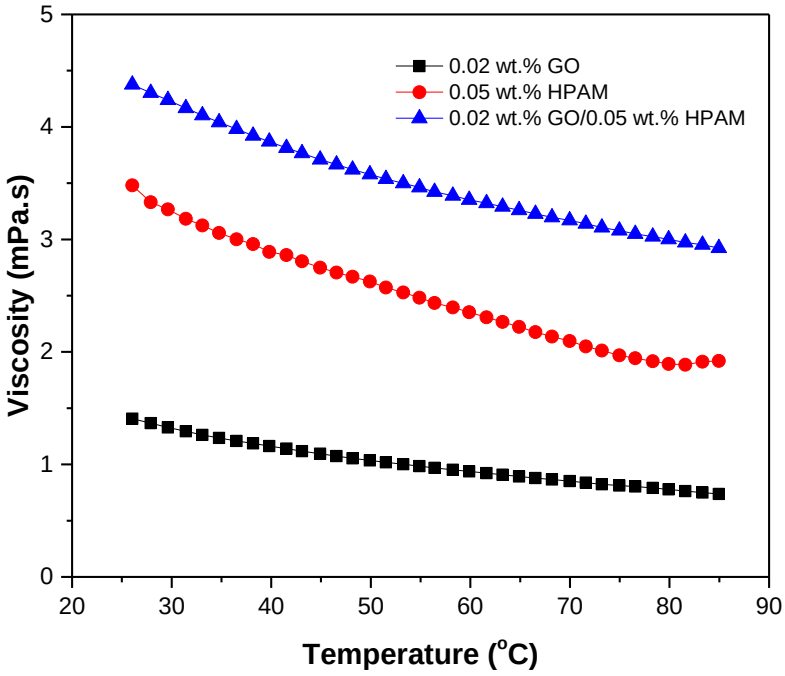

Figure 7. Comparison of the temperature effect on effective viscosities at a different temperature.

3.2.5. Long-term thermal stability of HPAM/GO composites

In industrial PF processes, the polymer is required to undergo long-term treatment under harsh conditions in the reservoir. Persistent ageing of the polymer under severe circumstances would cause viscosity reduction and hence drawbacks to the oil recovery [66]. The only available viscosity will serve as a primary benchmark for the injected polymer to reach the oil in the unfavourable environment.

Here, the influence of GO on ageing time is investigated. 0.05 wt. % HPAM and 0.0 5wt. % HPAM/0.1 wt. %GO Composites were examined at 80 °C, as illustrated in **Fig. 8**. The results indicate that the pure HPAM solution displayed less tolerance to ageing under harsh condition, while the composites containing HPAM/GO exhibited strong affinity to stay longer at the reservoir-like condition. It can be seen that the HPAM drop sharply after the five days showing less strength to withstand high temperature. Unlike pure HPAM, the viscosity of HPAM/GO composites dropped by only 4 % after the five days of ageing, and 6% after 30 days, whereas, HPAM viscosity reduction were up to 35 % after five days and almost 60% decrease was observed after 30 days. Such results are quite different to what was reported in the literature [13, 41], but similar to what we observed previously by using SiO_2/HPAM hybrid [24]. Both works shows that the nanocomposites have a strong ability to work under the harsh environmental condition, and could improve the HPAM stability while ageing. It is still unclear on the exact mechanism of stability reinforcement, which could be a result of inter-place among strengthened polymer molecular weight, ductility, and embrittlement due to the formation of covalent linkages and electrostatic hydrogen bonding between the GO and the HPAM functional groups, leading to enhanced material stability and hence more viscosity enhancement.

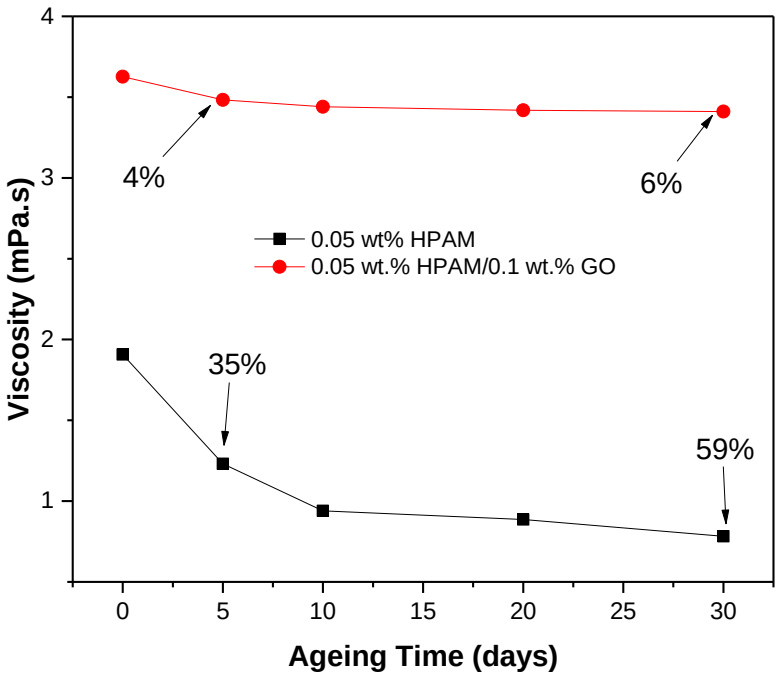

Figure 8. Long-term thermal stability to investigating the effect of ageing time (T=85 °C and shear rate 1000 s^{-1}) for 30 days.

3.2.6. Effect of electrolyte on the viscosity of HPAM/GO composites

Salinity tolerance is a significant factor in deteriorating the application of polymers in EOR processes. Since HPAM is regarded as a polyelectrolyte, its viscosity and hydrodynamic size are responsive to electrolyte concentration. In this study, the effect of electrolyte on the apparent viscosity of HPAM and the composite of HPAM/GO was investigated at 85 °C. It was observed from **Fig. 9** that for both HPAM and HPAM/GO composites, the addition of the NaCl from 1 to 8 wt. % decreases the viscosity, which is opposite to what was found in the literature [24, 67]. This is because when salt is added to the solution, the Na^+ can neutralise the negative charges of HPAM $-COO^-$ groups, reducing the polymer chains electrostatic repulsion, and therefore causing a conformational transition of the polymer to change from stretch to coiled or shrinkable state. Consequently, these lead to a reduction in the hydraulic radius and degree of entanglement of the polymer chain, which eventually decreases the viscosity. Furthermore, when HPAM is dissolved in water, the $-COO^-$ groups in the polymer chain repel each other causing its structure to remain extended, leading to high hydrodynamic volume to the molecular chain which increases the solution viscosity. It is, however, in a good agreement with the literature [41, 68] where a decrease in viscosity was observed at high salinities. For HPAM solution, it can also be seen that the viscosity continued to decrease until it reached a critical salinity threshold (CST) (i.e., above which the salinity has less or no effects on the viscosity). On the other hand, the HPAM/GO composites viscosities start to increase after it reaches CST. This is because the number of molecules to be shielded by the NaCl cations were limited. In this study, the critical salinity was found to be approximately 4 wt. % as shown in **Fig. 9.** This observation agrees with reports by Levitt et al. which indicated that above 3 wt. % NaCl concentration any variations in the HPAM viscosity is insignificant [69]. Additionally, the minor change at high salt concentration results due to the corresponding increase in the polarity of the solvents, which reinforced the intermolecular association of the hydrophobic groups, making the viscosity to remain stable. Also, in the presence of GO the insignificant influence of salt at high concentration can arise because most molecules of NaCl are already shrunk by the high proton concentration at a low NaCl content, therefore, after interacting with GO, the change in CST value is observed. It can be concluded that addition of the salt concentration into the polymer affects the viscosity of. HPAM significantly, HPAM/GO hybrid shows better capability of changing the CST, which could make the composites to be considered useful at high salt content compared to neat HPAM although the exact mechanism remains unclear.

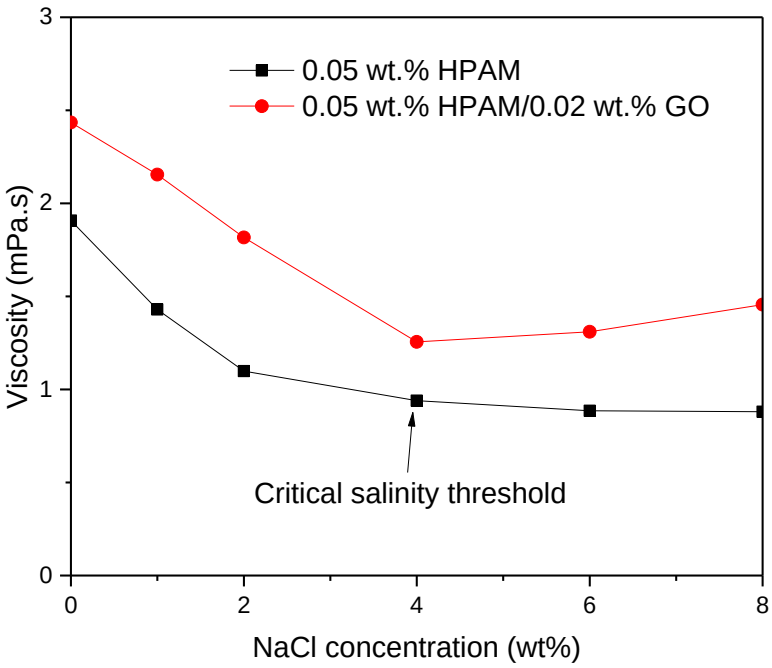

Figure 9. Influence of ionic strength on the average viscosity of HPAM and HPAM/GO composites (T=85 °C, shear rate 1000 s^{-1}).

3.2.7. Viscoelastic properties of HPAM/GO composites

The viscoelastic properties are mostly used to achieve a better perception of the deformation and molecular structure of the polymer(s), as their role in the EOR process is imperative [70-73]. Oscillatory tests were conducted in this work for pure HPAM and HPAM/GO composites. The results obtained for storage modulus (G') and loss modulus (G'') versus angular frequency (ω) are plotted. **Fig. 10a** shows the outcomes of dependency of loss factor on frequency (tan δ = G''/G') for both plain HPAM and the GO/HPAM nanocomposites. Precisely, with the addition of GO loading, a diminishing trend of tan δ was observed in the nanocomposite dispersions, indicating that when GO is incorporated into HPAM, it enhances elastic properties. Moreover, at highest GO content (0.1 wt. %) the value of tan δ was further decrease, and also shows a Newtonian character at lower angular frequency of 1–10 ($rads^{-1}$) and displaying behaviour relatively independent of frequency. The results in **Fig. 10b** shows a gradual increase in both elastic and loss modulus with the increasing angular frequency with the addition of GO, and continue to become more elastically dominant at highest GO concentration. Such trends are similar to what was reported in the literature [74]; some work also showed that GO improved the elasticity of polyacrylamide for dye adsorption capacity [75, 76]. At low frequency region, the plateau of G' indicate more obvious nature of an elastic material demonstrating solid-like character and gel network behaviour of nanofillers in polymer composites and colloidal gels [77-79] Moreover, the

results indicate that compared to the pure HPAM, the composites solutions possesses long-term relaxing time as a result of sufficient links and network structure between macromolecules. It can be concluded that the hybrids of HPAM/GO exhibit better viscoelastic strength. These indicate that the hybrid could have more ability to improve oil recovery under harsh reservoir conditions. The samples showed less frequency dependence behaviour in both G' and G'' indicating more solid-like than liquid-like viscoelastic nature particularly at high GO concentration. Therefore, the material with high GO loading displayed good behaviour, suggesting that the GO reduced the relaxation of the HPAM macromolecular chain, and hence the effect of liberation of the solution became less obvious, for example, at 0.1 wt. % GO, the G' increases by 59% and G'' increases by 63% respectively as compared to that of neat HPAM. This viscoelastic behaviour is similar to what was found in the studies about LDH/PAM and clay/polymer nanocomposites [74, 80].

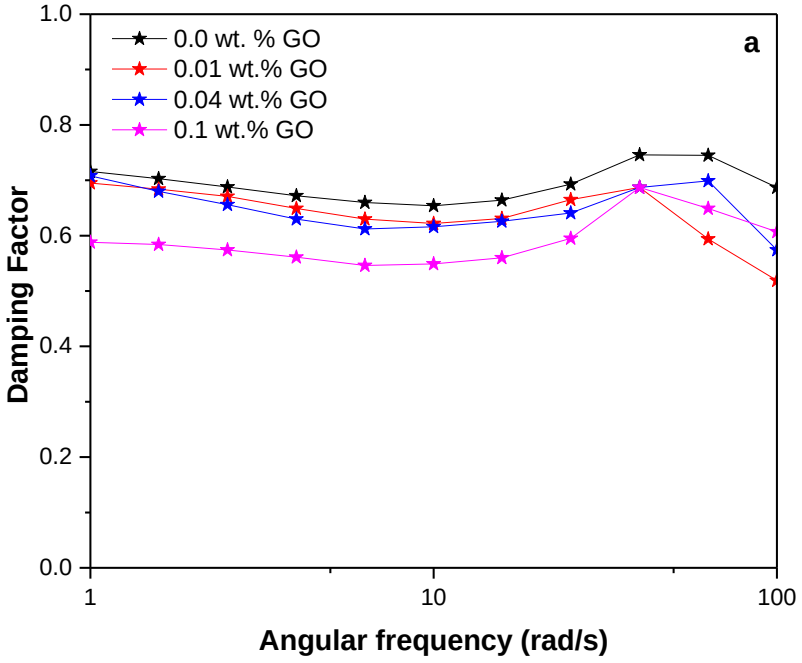

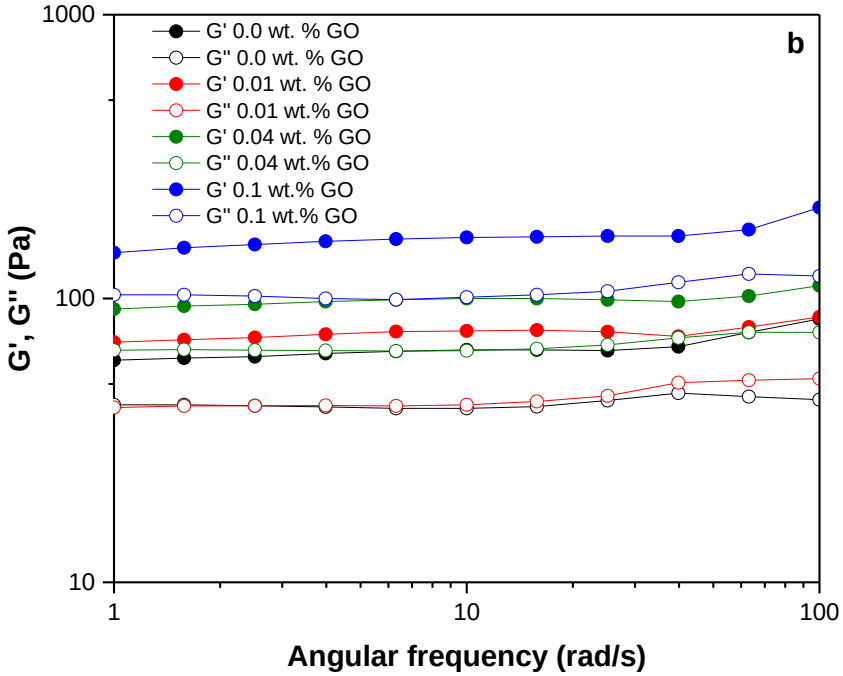

Figure 101. (a) Damping factor and (b) Storage modulus (G') and loss modulus (G'') for HPAM and HPAM with different GO concentrations as a function of angular frequency (ω).

4. CONCLUSION

The idea for the use of GO nanosheet to reinforce the high-temperature rheology and stability of HPAM was successfully demonstrated. The rheological behaviour of aqueous HAPM/GO composites was investigated. The composites show a rapid increase in viscosity and viscoelasticity compared to pure HPAM solution. The following outcomes can be drawn based on the results obtained:

- The FT-IR spectral data confirmed the formation of the hydrogen bonding between GO and HPAM functional groups, which helps to strengthen the hybrid stability.
- For pure HPAM, there is a critical association concentration (CAC) of 0.06 %， beyond which the viscosity increased significantly.
- The addition of different GO concentrations significantly increase the viscosity of the suspensions, and the effect is more significant at high temperatures. Addition of 0.1 wt. % of GO increased the viscosity by 47 % and 36 %, respectively, at 85°C and 25 °C.
- The addition of GO increased long-term thermal stability significantly due to the formation of electrostatic hydrogen bonding between the GO and the HPAM functional groups. After ageing for 30 days at 80 °C, the viscosity of the composites solution decreases very slightly while a 59 % reduction was observed for pure HPAM solution.

- Increasing the GO content increases both storage and loss modulus the HPAM solution, making them favourable for EOR applications
- Though the solution viscosity decreased with an increase in NaCl concentration for both HPAM and HPAM/GO composites, but the later improve the CST value showing promising performance at high salt content.

ACKNOWLEDGEMENT

The Authors acknowledge the support of the Petroleum Technology Development Funds (PTDF), Nigeria, and the European Research Council (ERC-2014-CoG, Project reference: 648375).

REFERENCES

1. Ghahremani, H., et al., *An experimental study of the performance of low-molecular weight polymer for enhanced heavy oil recovery in a heterogeneous media.* Geosystem Engineering, 2017: p. 1-8.
2. Sang, G., et al., *Biodegradation for hydrolyzed polyacrylamide in the anaerobic baffled reactor combined aeration tank.* Ecological engineering, 2015. **84**: p. 121-127.
3. Li, H., et al., *Novel polymer aids for low‐grade oil sand ore processing.* The Canadian Journal of Chemical Engineering, 2008. **86**(2): p. 168-176.
4. Ye, M., D. Han, and L. Shi, *Studies on determination of molecular weight for ultrahigh molecular weight partially hydrolyzed polyacrylamide.* Journal of applied polymer science, 1996. **60**(3): p. 317-322.
5. Lake, L., *W., 1989, Enhanced Oil Recovery*. 1989, Englewood Cliffs, New Jersey, USA: Prentice Hall.
6. Seright, R.S., et al., *Stability of partially hydrolyzed polyacrylamides at elevated temperatures in the absence of divalent cations.* Spe Journal, 2010. **15**(02): p. 341-348.
7. Erdlac Jr, R., et al. *Ongoing resource assessment of geothermal energy from sedimentary basins in Texas*. in *Proceedings, thirty-second workshop on geothermal reservoir engineering, Stanford University, Stanford, SGP-TR-183*. 2007.
8. Kopperud, H.M., F.K. Hansen, and B. Nyström, *Effect of surfactant and temperature on the rheological properties of aqueous solutions of unmodified and hydrophobically modified polyacrylamide.* Macromolecular Chemistry and Physics, 1998. **199**(11): p. 2385-2394.
9. Shaikh, S., et al., *Synthesis and solution properties of poly (acrylamide‐styrene) block copolymers with high hydrophobic content.* Polymer Engineering & Science, 1999. **39**(10): p. 1962-1968.
10. McCormick, C.L., T. Nonaka, and C.B. Johnson, *Water-soluble copolymers: 27. Synthesis and aqueous solution behaviour of associative acrylamideN-alkylacrylamide copolymers.* Polymer, 1988. **29**(4): p. 731-739.
11. Samanta, A., et al., *Effects of alkali, salts, and surfactant on rheological behavior of partially hydrolyzed polyacrylamide solutions.* Journal of Chemical & Engineering Data, 2010. **55**(10): p. 4315-4322.
12. Sabhapondit, A., A. Borthakur, and I. Haque, *Characterization of acrylamide polymers for enhanced oil recovery.* Journal of applied polymer science, 2003. **87**(12): p. 1869-1878.
13. Zhu, D., et al., *Aqueous hybrids of silica nanoparticles and hydrophobically associating hydrolyzed polyacrylamide used for EOR in high-temperature and high-salinity reservoirs.* Energies, 2014. **7**(6): p. 3858-3871.

14. Liu, Y., et al., *High clay content nanocomposite hydrogels with surprising mechanical strength and interesting deswelling kinetics.* Polymer, 2006. **47**(1): p. 1-5.
15. Sirousazar, M., et al., *Polyvinyl alcohol/Na-montmorillonite nanocomposite hydrogels prepared by freezing–thawing method: Structural, mechanical, thermal, and swelling properties.* Journal of Macromolecular Science, Part B, 2012. **51**(7): p. 1335-1350.
16. Haraguchi, K. and T. Takehisa, *Nanocomposite hydrogels: a unique organic-inorganic network structure with extraordinary mechanical, optical, and swelling/de-swelling properties.* Advanced Materials, 2002. **14**(16): p. 1120.
17. Tongwa, P., R. Nygaard, and B. Bai, *Evaluation of a nanocomposite hydrogel for water shut‐off in enhanced oil recovery applications: Design, synthesis, and characterization.* Journal of Applied Polymer Science, 2013. **128**(1): p. 787-794.
18. Okay, O. and W. Oppermann, *Polyacrylamide− Clay Nanocomposite Hydrogels: Rheological and Light Scattering Characterization.* Macromolecules, 2007. **40**(9): p. 3378-3387.
19. Aalaie, J., et al., *Effect of montmorillonite on gelation and swelling behavior of sulfonated polyacrylamide nanocomposite hydrogels in electrolyte solutions.* European Polymer Journal, 2008. **44**(7): p. 2024-2031.
20. Aalaie, J. and M. Youssefi, *Study on the dynamic rheometry and swelling properties of the polyacrylamide/laponite nanocomposite hydrogels in electrolyte media.* Journal of Macromolecular Science, Part B, 2012. **51**(6): p. 1027-1040.
21. Hu, G., et al., *Low percolation thresholds of electrical conductivity and rheology in poly (ethylene terephthalate) through the networks of multi-walled carbon nanotubes.* Polymer, 2006. **47**(1): p. 480-488.
22. Xu, G., et al., *Rheology of a low‐filled polyamide 6/montmorillonite nanocomposite.* Journal of applied polymer science, 2008. **108**(3): p. 1501-1505.
23. Saito, Y., H. Ogura, and Y. Otsubo, *Rheological behavior of silica suspensions in aqueous solutions of associating polymer.* Colloid and polymer science, 2008. **286**(13): p. 1537.
24. Hu, Z., et al., *Rheological Properties of Partially Hydrolyzed Polyacrylamide Seeded by Nanoparticles.* Industrial & Engineering Chemistry Research, 2017. **56**(12): p. 3456-3463.
25. Maghzi, A., et al., *The impact of silica nanoparticles on the performance of polymer solution in presence of salts in polymer flooding for heavy oil recovery.* Fuel, 2014. **123**: p. 123-132.
26. Giraldo, L.J., et al., *The effects of SiO2 nanoparticles on the thermal stability and rheological behavior of hydrolyzed polyacrylamide based polymeric solutions.* Journal of Petroleum Science and Engineering, 2017. **159**: p. 841-852.
27. Zhang, L., T. Tao, and C. Li, *Formation of polymer/carbon nanotubes nano-hybrid shish–kebab via non-isothermal crystallization.* Polymer, 2009. **50**(15): p. 3835-3840.
28. Nourafkan, E., et al., *Synthesis of stable iron oxide nanoparticle dispersions in high ionic media.* Journal of Industrial and Engineering Chemistry, 2017. **50**: p. 57-71.
29. Fu, P., et al., *Preparation, stability and rheology of polyacrylamide/pristine layered double hydroxide nanocomposites.* Journal of Materials Chemistry, 2010. **20**(19): p. 3869-3876.
30. Hu, Z. and G. Chen, *Novel nanocomposite hydrogels consisting of layered double hydroxide with ultrahigh tensibility and hierarchical porous structure at low inorganic content.* Advanced Materials, 2014. **26**(34): p. 5950-5956.
31. Tjong, S.C., *Structural and mechanical properties of polymer nanocomposites.* Materials Science and Engineering: R: Reports, 2006. **53**(3): p. 73-197.
32. Geim, A.K. and K.S. Novoselov, *The rise of graphene.* Nature materials, 2007. **6**(3): p. 183.
33. Liu, R., et al., *Tough and highly stretchable graphene oxide/polyacrylamide nanocomposite hydrogels.* Journal of Materials Chemistry, 2012. **22**(28): p. 14160-14167.
34. Shen, J., et al., *Study on graphene-oxide-based polyacrylamide composite hydrogels.* Composites Part A: Applied Science and Manufacturing, 2012. **43**(9): p. 1476-1481.
35. Bai, H., et al., *Graphene oxide/conducting polymer composite hydrogels.* Journal of Materials Chemistry, 2011. **21**(46): p. 18653-18658.

36. Potts, J.R., et al., *Graphene-based polymer nanocomposites.* Polymer, 2011. **52**(1): p. 5-25.
37. Fan, J., et al., *Glycidyl methacrylate-modified gum arabic mediated graphene exfoliation and its use for enhancing mechanical performance of hydrogel.* Polymer, 2013. **54**(15): p. 3921-3930.
38. Nguyen, B.D., et al., *The impact of graphene oxide particles on viscosity stabilization for diluted polymer solutions using in enhanced oil recovery at HTHP offshore reservoirs.* Advances in Natural Sciences: Nanoscience and Nanotechnology, 2014. **6**(1): p. 015012.
39. Rodewald, P.G., *Oil recovery by waterflooding employing graphite oxide for mobility control*. 1976, Google Patents.
40. Oberdisse, J., *Aggregation of colloidal nanoparticles in polymer matrices.* Soft matter, 2006. **2**(1): p. 29-36.
41. Zhu, D., et al., *Enhancing rheological properties of hydrophobically associative polyacrylamide aqueous solutions by hybriding with silica nanoparticles.* Journal of Applied Polymer Science, 2014. **131**(19).
42. Zhao, X., et al., *Enhanced mechanical properties of graphene-based poly (vinyl alcohol) composites.* Macromolecules, 2010. **43**(5): p. 2357-2363.
43. Zhang, H., D. Zhai, and Y. He, *Graphene oxide/polyacrylamide/carboxymethyl cellulose sodium nanocomposite hydrogel with enhanced mechanical strength: preparation, characterization and the swelling behavior.* RSC Advances, 2014. **4**(84): p. 44600-44609.
44. Hummers Jr, W.S. and R.E. Offeman, *Preparation of graphitic oxide.* Journal of the american chemical society, 1958. **80**(6): p. 1339-1339.
45. Hebishy, E., et al., *Physical and oxidative stability of whey protein oil-in-water emulsions produced by conventional and ultra high-pressure homogenization: Effects of pressure and protein concentration on emulsion characteristics.* Innovative Food Science & Emerging Technologies, 2015. **32**: p. 79-90.
46. Wu, J., et al., *Solvothermal synthesis and characterization of sandwich-like graphene/ZnO nanocomposites.* Applied Surface Science, 2010. **256**(9): p. 2826-2830.
47. Cai, D. and M. Song, *Preparation of fully exfoliated graphite oxide nanoplatelets in organic solvents.* Journal of Materials Chemistry, 2007. **17**(35): p. 3678-3680.
48. Srivastava, S., et al., *Faster response of NO2 sensing in graphene–WO3 nanocomposites.* Nanotechnology, 2012. **23**(20): p. 205501.
49. Wang, G., et al., *Facile Synthesis and Characterization of Graphene Nanosheets.* The Journal of Physical Chemistry C, 2008. **112**(22): p. 8192-8195.
50. Yi, M., et al., *Achieving concentrated graphene dispersions in water/acetone mixtures by the strategy of tailoring Hansen solubility parameters.* Journal of Physics D: Applied Physics, 2012. **46**(2): p. 025301.
51. Guerrero-Contreras, J. and F. Caballero-Briones, *Graphene oxide powders with different oxidation degree, prepared by synthesis variations of the Hummers method.* Materials Chemistry and Physics, 2015. **153**: p. 209-220.
52. An, Y.-X., et al., *The assembly of a composite based on nano-sheet graphene oxide and montmorillonite.* Petroleum Science: p. 1-9.
53. Ni, Y., et al., *Preparation, characterization, and optical, electrochemical property research of CdS/PAM nanocomposites.* The Journal of Physical Chemistry B, 2006. **110**(35): p. 17347-17352.
54. Cheng, Q.-Y., et al., *Supramolecular self-assembly induced graphene oxide based hydrogels and organogels.* Langmuir, 2012. **28**(5): p. 3005-3010.
55. Wang, X., D. Hu, and J. Yang, *Synthesis of PAM/TiO2 composite microspheres with hierarchical surface morphologies.* Chemistry of materials, 2007. **19**(10): p. 2610-2621.
56. Gao, H., et al., *Bifunctional ultraviolet/ultrasound responsive composite TiO 2/polyelectrolyte microcapsules.* Nanoscale, 2016. **8**(9): p. 5170-5180.
57. Kavitha, T., S.I.H. Abdi, and S.-Y. Park, *pH-sensitive nanocargo based on smart polymer functionalized graphene oxide for site-specific drug delivery.* Physical Chemistry Chemical Physics, 2013. **15**(14): p. 5176-5185.

58. Kejun, Y. and Z. Guowei, *Synthesis and rheological properties in aqueous solution of poly (acrylamide‐co‐sodium allylsulfonate).* Journal of applied polymer science, 1992. **44**(1): p. 1-7.
59. Chen, W., et al., *Fabricating a flocculant with controllable cationic microblock structure: characterization and sludge conditioning behavior evaluation.* Industrial & Engineering Chemistry Research, 2016. **55**(10): p. 2892-2902.
60. Phuoc, T.X., M. Massoudi, and R.-H. Chen, *Viscosity and thermal conductivity of nanofluids containing multi-walled carbon nanotubes stabilized by chitosan.* International Journal of Thermal Sciences, 2011. **50**(1): p. 12-18.
61. Teng, T.-P., L. Lin, and C.-C. Yu, *Preparation and characterization of carbon nanofluids by using a revised water-assisted synthesis method.* Journal of Nanomaterials, 2013. **2013**: p. 133.
62. Li, X., D. Zhu, and X. Wang, *Evaluation on dispersion behavior of the aqueous copper nano-suspensions.* Journal of colloid and interface science, 2007. **310**(2): p. 456-463.
63. Chen, Y., et al., *Mechanically strong and pH-responsive carboxymethyl chitosan/graphene oxide/polyacrylamide nanocomposite hydrogels with fast recoverability.* Journal of Biomaterials Science, Polymer Edition, 2017. **28**(16): p. 1899-1917.
64. Yeo, S.-D., I.-S. Kang, and E. Kiran, *Critical polymer concentrations of polyethylene solutions in pentane.* Journal of Chemical & Engineering Data, 2002. **47**(3): p. 571-574.
65. Grassl, B., et al., *Poly (ethylene oxide)‐and poly (acrylamide)‐based water‐soluble associative polymers: synthesis, characterisation, properties in solution.* Polymer international, 2006. **55**(10): p. 1169-1176.
66. Pospíšil, J., et al., *Degradation and aging of polymer blends I. Thermomechanical and thermal degradation.* Polymer Degradation and Stability, 1999. **65**(3): p. 405-414.
67. Feng, Y., et al., *Hydrophobically associating polyacrylamides and their partially hydrolyzed derivatives prepared by post-modification. 2. Properties of non-hydrolyzed polymers in pure water and brine.* Polymer, 2005. **46**(22): p. 9283-9295.
68. Jung, J.C., et al., *Rheology and polymer flooding characteristics of partially hydrolyzed polyacrylamide for enhanced heavy oil recovery.* Journal of Applied Polymer Science, 2013. **127**(6): p. 4833-4839.
69. Levitt, D. and G.A. Pope. *Selection and screening of polymers for enhanced-oil recovery*. in *SPE Symposium on Improved Oil Recovery*. 2008. Society of Petroleum Engineers.
70. Mitchell, J., et al., *Viscoelastic polymer flows and elastic turbulence in three-dimensional porous structures.* Soft matter, 2016. **12**(2): p. 460-468.
71. Spildo, K. and E.I. Sæ, *Effect of Charge Distribution on the Viscosity and Viscoelastic Properties of Partially Hydrolyzed Polyacrylamide.* Energy & Fuels, 2015. **29**(9): p. 5609-5617.
72. Wei, B., *Flow characteristics of three enhanced oil recovery polymers in porous media.* Journal of Applied Polymer Science, 2015. **132**(10).
73. ZHANG, L.-j. and X.-a. Yue, *Mechanism for viscoelastic polymer solution percolating through porous media.* Journal of Hydrodynamics, Ser. B, 2007. **19**(2): p. 241-248.
74. Hu, Z. and G. Chen, *Aqueous dispersions of layered double hydroxide/polyacrylamide nanocomposites: preparation and rheology.* Journal of Materials Chemistry A, 2014. **2**(33): p. 13593-13601.
75. Fan, J., et al., *Mechanically strong graphene oxide/sodium alginate/polyacrylamide nanocomposite hydrogel with improved dye adsorption capacity.* Journal of Materials Chemistry A, 2013. **1**(25): p. 7433-7443.
76. Yang, Y., S. Song, and Z. Zhao, *Graphene oxide (GO)/polyacrylamide (PAM) composite hydrogels as efficient cationic dye adsorbents.* Colloids and Surfaces A: Physicochemical and Engineering Aspects, 2017. **513**: p. 315-324.
77. Imperiali, L., et al., *A simple route towards graphene oxide frameworks.* Materials Horizons, 2014. **1**(1): p. 139-145.

78. Song, Y., C. Xu, and Q. Zheng, *Styrene–butadiene–styrene copolymer compatibilized carbon black/polypropylene/polystyrene composites with tunable morphology, electrical conduction and rheological stabilities.* Soft Matter, 2014. **10**(15): p. 2685-2692.
79. Bai, L., et al., *Localizing graphene at the interface of cocontinuous polymer blends: Morphology, rheology, and conductivity of cocontinuous conductive polymer composites.* Journal of Rheology, 2017. **61**(4): p. 575-587.
80. Lepoittevin, B., et al., *Poly (ε-caprolactone)/clay nanocomposites prepared by melt intercalation: mechanical, thermal and rheological properties.* Polymer, 2002. **43**(14): p. 4017-4023.